Vibrational energies for NH_3 based on high level ab initio potential energy surfaces

Hai Lin, Walter Thiel, Sergei N. Yurchenko, Miguel Carvajal, and Per Jensen

Citation: J. Chem. Phys. **117**, 11265 (2002); doi: 10.1063/1.1521762
View online: https://doi.org/10.1063/1.1521762
View Table of Contents: http://aip.scitation.org/toc/jcp/117/24
Published by the American Institute of Physics

Vibrational energies for NH_3 based on high level *ab initio* potential energy surfaces

Hai Lin and Walter Thiel[a)]
Max-Planck-Institut für Kohlenforschung, Kaiser-Wilhelm-Platz 1, D-45470 Mülheim an der Ruhr, Germany

Sergei N. Yurchenko, Miguel Carvajal, and Per Jensen[b)]
Theoretische Chemie, Fachbereich 9, Bergische Universität-Gesamthochschule Wuppertal, D-42097 Wuppertal, Germany

(Received 7 August 2002; accepted 24 September 2002)

Ab initio coupled cluster calculations with single and double substitutions and a perturbative treatment of connected triple substitutions [CCSD(T)] have been carried out to generate six-dimensional (6D) potential energy surfaces (PES) and dipole moment surfaces (DMS) for the electronic ground state of ammonia. Full 6D-PES and 6D-DMS (14400 points) were computed with the augmented correlation-consistent triple-zeta basis (aug-cc-pVTZ). For a selected number of points (420 in C_{3v} symmetry and 1260 in lower symmetry), more accurate energies (CBS+) were obtained by extrapolating the CCSD(T) results for the aug-cc-pVXZ (X=T,Q,5) basis sets to the complete basis set limit and adding corrections for core-valence correlation and relativistic effects. Two procedures were investigated to enhance the quality of the 6D-PES from CCSD(T)/aug-cc-pVTZ by including the CBS+ data points. The resulting 6D-PES were represented by analytical functions involving Morse variables for the stretches, symmetry-adapted bending coordinates, and a specially designed inversion coordinate (up to 76 fitted parameters, rms deviations of about 5 cm^{-1} for 14 400 *ab initio* data points). For these analytical surfaces, vibrational energies were calculated with a newly developed computer program using a variational model that employs an Eckart-frame kinetic energy operator. Results are presented and compared to experiment for the vibrational band centers of NH_3 and its isotopomers up to around 15 000 cm^{-1}. For our best 6D-PES, the term values of the fundamentals are reproduced with rms deviations of 4.4 cm^{-1} (NH_3) and 2.6 cm^{-1} (all isotopomers), the maximum deviation being 7.9 cm^{-1}. © *2002 American Institute of Physics.* [DOI: 10.1063/1.1521762]

I. INTRODUCTION

Ammonia is a textbook example of a nonrigid molecule,[1] i.e., a molecule capable of tunneling between multiple minima on its potential energy surface. In the NH_3 molecule, the tunneling motion is an inversion during which the molecule flips, much like an umbrella flipping over in stormy weather, between two equivalent configurations that are mirror images of each other. This large amplitude vibration causes the rotation-vibration energy levels of NH_3 to exhibit inversion splittings which are easily detectable in the rotation-vibration spectra. Owing to the nonrigidity of ammonia, its intramolecular dynamics has been extensively studied. In addition to this more academic interest, ammonia is an important molecule in an astrophysical context. It is the fourth most abundant constituent in the atmospheres of Jupiter and Saturn and spectral assignments are useful to determine atmospheric temperatures.[2,3]

Due to the large amplitude vibration, the accurate calculation of the rotation-vibration energies of the ammonia molecule directly from the potential energy function is a challenging problem which has been addressed a number of times (see, for example, Refs. 4–6). In the present work, we calculate *ab initio* potential energy surfaces for the electronic ground state of NH_3, and from these surfaces we compute vibrational energies by means of a newly developed computer program. The vibrational calculation is variational but employs an Eckart-frame kinetic energy operator (see, for example, Ref. 1). We intend to develop this theoretical model further to describe the rotational motion, and the Eckart-frame approach is chosen in order to minimize rotation-vibration coupling and thus facilitate the accurate calculation of highly excited rotational states.

Many *ab initio* studies have been concerned with the inversion barrier of ammonia. The most recent high-level calculations[7,8] employ coupled cluster theory [CCSD(T)] with extrapolation to the complete basis set (CBS) limit and further corrections to arrive at adiabatic equilibrium barriers of 1758 and 1777 cm^{-1}, respectively. By contrast, only a few *ab initio* potential energy surfaces (PES) have been published for ammonia. An early analytic surface[4] was determined from experimental rovibrational transition data with the use of some *ab initio* force constants in the fitting procedure. A complete quartic force field was computed at the CCSD(T) level (basis sets: cc-pVTZ, cc-pVQZ) and used to derive spectroscopic constants by rovibrational perturbation theory.[9] This force field refers to the equilibrium structure of ammonia and therefore it cannot describe correctly the inversion motion.[10] More recently, two-dimensional potential en-

a)Electronic mail: thiel@mpi-muelheim.mpg.de
b)Author to whom correspondence should be addressed. Electronic mail: jensen@uni-wuppertal.de

ergy surfaces for totally symmetric motions were generated by CCSD(T) calculations (basis sets: aug-cc-pVTZ, cc-pVQZ, aug-cc-pVQZ) and employed in variational calculations which led to very good agreement with experiment for the 22 inversion levels studied.[5] Finally, a full six-dimensional potential energy surface was determined by density functional theory with the B97-1 functional (basis set: TZ2P) and used in three different variational treatments which yield similar vibrational energies and reproduce the experimental fundamental wave numbers to within 15 cm^{-1}.[6]

As mentioned previously, this paper presents variational calculations of the vibrational energies of ammonia with particular emphasis on the inversion process. They are based on full six-dimensional potential energy surfaces evaluated at the CCSD(T) level that are more complete and more accurate than other theoretical surfaces published previously (14 400 points from CCSD(T)/aug-cc-pVTZ enhanced by data with complete basis extrapolation and further corrections). In the following, we describe the computation of the *ab initio* surfaces (Sec. II), their representation by analytical functions (Secs. III–IV), and the vibrational energy calculations (Sec. V).

II. *AB INITIO* CALCULATIONS

A. Computational scheme

All quantum-chemical calculations were carried out at the CCSD(T) level (coupled cluster theory with all single and double substitutions from the Hartree–Fock reference determinant[11] augmented by a perturbative treatment of connected triple excitations[12,13]) using the MOLPRO2000 package.[14,15] The correlation-consistent families of basis sets cc-pVXZ, aug-cc-pVXZ, and aug-cc-pCVXZ (X=T,Q,5) developed by Dunning and co-workers[16,17] were employed. For brevity, we denote the CCSD(T) calculations with the cc-pVXZ, aug-cc-pVXZ, and aug-cc-pCVXZ basis sets by XZ, AXZ, and ACXZ, respectively. According to whether the frozen core approximation was applied or not, ''fc'' or ''cc'' is added to the notation. Default thresholds from MOLPRO2000 were used unless noted otherwise.[18]

To reach the complete basis set (CBS) limit, AXZfc (X=T,Q,5) energies were calculated and extrapolated according to[19]

$$E = E_{\mathrm{extra}} + b/X^3, \tag{1}$$

where b is a fit parameter and X=3,4,5 now denotes the cardinal quantum number of the basis set. An alternative procedure[7] employs separate extrapolations of the Hartree–Fock energy by an exponential ansatz[20] and of the CCSD(T) correlation energy according to Eq. (1). We have tested both procedures and find that they yield essentially identical results in our case. Therefore we have only used the first approach.[19]

The extrapolated total energies from Eq. (1) (E_{extra}) can be corrected for core–valence correlation and relativistic effects. The core–valence correlation contribution (E_{core}) was obtained as the energy difference between frozen-core (ACTZfc) and all-electron (ACTZcc) calculations. The scalar relativistic correction (E_{rel}) was evaluated at the ATZfc level as the sum of the expectation values for the mass–velocity and the one-electron Darwin terms (typical values around 0.115 and −0.144 a.u., significant cancellation). The final corrected energy (E_{corr}) is given by $E_{\mathrm{corr}} = E_{\mathrm{extra}} + E_{\mathrm{core}} + E_{\mathrm{rel}}$.

Geometries were optimized for a variety of basis sets using a gradient convergence criterion of 0.000 01 a.u. so that the resulting bond lengths and angles are expected to be precise to about 0.000 01 Bohr and 0.001°. Potential energy surfaces (PES) were generated at five levels: ATZfc, AQZfc, A5Zfc, CBS (E_{extra}), and CBS+ (E_{corr}). We employed the same grid at all levels (see below), and therefore defined the grid in terms of bond lengths and angles rather than displacement coordinates. Dipole moment surfaces (DMS) were only computed at the ATZfc level using a numerical finite-difference procedure with an added dipole field of 0.005 a.u.

B. Optimized geometry and inversion barrier

Table I lists optimized geometries and inversion barriers that have been obtained without any extrapolations or corrections. We confirm previous experience that the N–H bond length converges in an irregular pattern due to basis set superposition errors in XZ calculations,[21] whereas the AXZ and ACXZ results converge more smoothly upon basis set extension. For some basis sets, the optimized geometries in Table I can be compared with recent literature values[5,7,8] which are reproduced within the expected precision (see above).

In Table I the AC5Zcc calculations should be most reliable since they employ the largest basis set and include an explicit treatment of core–valence correlation. Our best directly computed inversion barrier is therefore 1783.5 cm^{-1}. The AC5Zcc equilibrium geometry (R=1.0109 Å, α=106.77°) is well reproduced by other calculations with large basis sets, in particular by AQZcc (deviations of only 0.0002 Å and 0.04°). The dipole moments at various optimized geometries were also computed at the ATZfc level and are given in Table I as the last column. Only the M_z component along the C_3 axis was calculated, since the other components are zero by symmetry.

Table II compares the inversion barriers derived from the current and previous[7,8] work. Basis set extension and core–valence correlation obviously tend to lower the barrier while relativistic corrections yield a slight increase. Our extrapolated CCSD(T) barrier of 1821 cm^{-1} lies close to and between analogous previous values.[7,8] The core–valence correction of −50 cm^{-1} is somewhat less negative than found previously,[7,8] and the relativistic correction of 18 cm^{-1} is also slightly smaller. These corrections lead to an estimate (E_{corr}) for the barrier of 1790 cm^{-1}. Using a more accurate core–valence correction of −64 cm^{-1} (see footnote d of Table II) and adding a diagonal Born–Oppenheimer correction[8] of −10 cm^{-1} would shift this value to 1766 cm^{-1}, close to the final estimates of 1758 cm^{-1} from Ref. 7 and of 1777 cm^{-1} from Ref. 8.

TABLE I. Optimized geometries, inversion barriers, and dipole moments at the CCSD(T) level for NH_3.[a]

	C_{3v}			D_{3h}				
Method	E/a.u.	R_{NH}/Å	α_{HNH}/deg	E/a.u.	R_{NH}/Å	α_{HNH}/deg	E_{inv}/cm^{-1}	M_z/Debye[b]
DZfc	−56.402 802 2	1.027 287	103.537	−56.388 657 2	1.005 150	120.000	3104.5	−1.632 695 9
TZfc	−56.473 197 2	1.014 128	105.644	−56.463 000 8	0.995 238	120.000	2237.9	−1.554 045 4
QZfc	−56.493 053 2	1.012 455	106.183	−56.483 823 6	0.994 900	120.000	2025.7	−1.531 050 1
5Zfc	−56.499 451 2	1.012 090	106.514	−56.490 822 0	0.995 233	120.000	1893.9	−1.516 195 7
ATZfc	−56.480 562 7	1.014 898	106.401	−56.471 739 3	0.997 529	120.000	1936.5	−1.519 805 6
AQZfc	−56.495 732 6	1.012 823	106.537	−56.487 226 1	0.996 024	120.000	1867.0	−1.514 714 6
A5Zfc	−56.500 284 2	1.012 291	106.580	−56.491 866 1	0.995 597	120.000	1847.6	−1.508 312 9
ATZcc	−56.497 886 5	1.012 014	106.686	−56.489 630 6	0.995 217	120.000	1812.0	−1.507 090 8
AQZcc	−56.527 293 9	1.010 688	106.727	−56.519 012 9	0.994 489	120.000	1817.5	−1.513 048 3
A5Zcc	−56.538 421 3	1.009 815	106.776	−56.530 160 9	0.993 689	120.000	1812.9	−1.505 293 4
AC5Zcc	−56.559 220 3	1.010 904	106.769	−56.551 094 3	0.994 593	120.000	1783.5	−1.505 028 8

[a]The (aug)-cc-p(C)VXZ basis set is denoted as (A)(C)XZ. Notations "fc" and "cc" correspond to frozen-core and all-electron calculations. See text for details.
[b]ATZfc level calculations for the C_{3v} geometries.

C. Potential energy and dipole moment surfaces

The one-dimensional (1D) PES was explored as the inversion potential from planarity through the minimum out to a well-bent geometry. The minimum energy path for inversion was determined by optimizing the N–H bond length for each HNH angle. Three kinds of 1D PES are reported in Table III. The first one (1D-ATZfc) was calculated at the ATZfc level through geometry optimizations. The second one (1D-CBS) and the third one (1D-CBS+) were determined from the corresponding theoretical 2D PES (see below) as follows:[22] For a given angle, the energies at various bond lengths were interpolated using cubic splines, and the minimum was then located by fitting the interpolated (11) data points near the minimum to a parabola.

C_{3v} (or D_{3h}) symmetry was maintained when generating the 2D PES. The grid was set up with 21 distances R_{NH} between 0.60 and 1.65 Å and 20 angles α_{HNH} between 70° and 120°. The data points were more dense in the vicinity of the equilibrium geometry and the saddle point.[23] In total 420 data points were computed. The 2D PES were first obtained at the ATZfc, AQZfc, and A5Zfc levels, and those at the CBS and CBS+ levels were determined afterwards (see Sec. II A). The 2D DMS was generated on the same grid at the ATZfc level.

Six-dimensional (6D) PES were determined on three grids. The first one (6D-1) was generated by varying all bond lengths and angles in the range R_{NH} =[0.85,0.90,0.95,0.99,1.01,1.05,1.10,1.20] Å and α_{HNH} =[120,116,112,108,104,100,90,80] deg. This large grid produced 14 400 data points. The ATZfc level was chosen for this PES to limit the computational effort. The corresponding 6D DMS was also computed for this large grid.

The second grid (6D-2) employed 560 data points close to the equilibrium geometry. In this case, the variables cover the range R_{NH}=[0.99,1.01,1.05] Å and α_{HNH} =[120,116,112,108,104,98] deg, respectively. Similar to the 2D case, five PES were computed at the ATZfc, AQZfc, A5Zfc, CBS, and CBS+ levels.

The third grid (6D-3) extends over the same region as the first one (6D-1) but is considerably sparser: R_{NH}=[0.85,0.99,1.05,1.20] Å and α_{HNH} =[120,112,101,90,80] deg. At the corresponding 700 data points, potential energy surfaces were again calculated at the ATZfc, AQZfc, A5Zfc, CBS, and CBS+ levels. The differences between the CBS+ and ATZfc energies at these 700 points were interpolated employing cubic polynomials which allowed us to determine corrections to the ATZfc energies of all 14 400 points on the large (6D-1) grid. Adding these cor-

TABLE II. Inversion barrier of NH_3.[a]

	This work		Ref. 7		Ref. 8	
Contribution	Theory/basis	E/cm^{-1}	Theory/basis	E/cm^{-1}	Theory/basis	E/cm^{-1}
Extra.	CCSD(T)/AXZ	1821[b]	MP2/XZ,CCSD(T)/XZ	1810	CCSD(T)/(A)XZ,CCSD(T)-R12/B	1831
Core corr.	CCSD(T)/ACTZ	−50[c,d]	MP2/CQZ	−64	MP2/CQZ,CCSD(T)-R12/B	−64
Relat. corr.	CCSD(T)/ATZ	18[c]	MP2/TZ	23	HF/YZ,CCSD(T)/YZ,HF/u-CYZ	20
BO corr.	no	⋯	yes	−11	yes	−10
Sum		1790		1758		1777

[a]Barriers after extrapolation to the CBS limit, core-valence correlation corrections, scalar relativistic corrections, and diagonal Born–Oppenheimer (BO) corrections are listed. For extrapolation, X=T,Q,5 in this work, X=Q,5,6 in Refs. 7, 8 and Y=D,T,Q in Ref. 8. See text and also the cited literature for details.
[b]Two-point extrapolation with X=Q,5 yields 1827 cm^{-1}.
[c]Evaluated at the AC5Zcc geometry. Essentially the same results are obtained at other high-level geometries (A5Zfc, AQZcc, A5Zcc).
[d]The CCSD(T)/A5Zfc and CCSD(T)/AC5Zcc barriers obtained from individually optimized geometries (Table I) imply a core–valence correlation correction of −64 cm^{-1}, in complete agreement with previous work (Refs. 7, 8). We quote the less accurate correction from CCSD(T)/A(C)TZ for the sake of consistency, since our PES calculations employ this level for the core–valence correlation correction (see Sec. II A).

TABLE III. Inversion potential for NH_3.[a]

	1D-ATZfc		1D-CBS		1D-CBS+	
α_{HNH}/deg	R_{NH}/Å	E/a.u.	R_{NH}/Å	E/a.u.	R_{NH}/Å	E/a.u.
120.000	0.997 529	−56.471 739 3	0.994 989	−56.497 731 3	0.993 985	−56.578 654 5
119.000	0.998 833	−56.472 961 8	0.996 262	−56.498 861 7	0.995 264	−56.579 770 5
118.000	1.000 129	−56.474 093 0	0.997 534	−56.499 962 5	0.996 530	−56.580 841 9
116.000	1.002 701	−56.476 091 4	1.000 023	−56.501 831 1	0.999 037	−56.582 735 6
114.000	1.005 254	−56.477 735 4	1.002 469	−56.503 403 3	1.001 484	−56.584 272 4
112.000	1.007 796	−56.479 014 8	1.004 863	−56.504 623 9	1.003 886	−56.585 473 1
110.000	1.010 331	−56.479 918 0	1.007 224	−56.505 499 3	1.006 249	−56.586 282 9
109.000	1.011 599	−56.480 225 2	1.008 383	−56.505 752 4	1.007 410	−56.586 552 9
108.000	1.012 867	−56.480 434 5	1.009 515	−56.505 967 0	1.008 573	−56.586 723 2
107.000	1.014 137	−56.480 544 6	1.010 818	−56.506 020 1	1.009 727	−56.586 824 3
106.000	1.015 409	−56.480 554 5	1.012 118	−56.506 012 1	1.011 039	−56.586 810 3
105.000	1.016 685	−56.480 463 1	1.013 414	−56.505 874 6	1.012 334	−56.586 650 7
104.000	1.017 967	−56.480 269 4	1.014 713	−56.505 691 7	1.013 640	−56.586 453 7
103.000	1.019 254	−56.479 972 4	1.016 007	−56.505 379 1	1.014 937	−56.586 104 0
101.000	1.021 852	−56.479 064 5	1.018 589	−56.504 426 2	1.017 532	−56.585 153 9
99.000	1.024 492	−56.477 731 1	1.021 174	−56.503 025 2	1.020 136	−56.583 756 2
95.000	1.029 952	−56.473 754 3	1.026 417	−56.498 919 0	1.025 404	−56.579 617 2
90.000	1.037 275	−56.466 231 3	1.033 700	−56.491 334 1	1.032 594	−56.571 969 2
80.000	1.054 695	−56.442 077 4	1.050 918	−56.466 737 0	1.049 804	−56.547 350 7
70.000	1.078 830	−56.404 424 9	1.075 125	−56.428 651 4	1.074 026	−56.509 094 1

[a]1D PES, C_{3v} or D_{3h} symmetry, bond lengths optimized. See text for details.

rections to the ATZfc energies yields an interpolated high-level surface on the large grid that is denoted by 6D-1-CBS*. By construction, the CBS+ energies on the 6D-3 grid (700 points) are reproduced by this surface. Its quality can further be checked through comparisons with the available CBS+ energies on the 2D and 6D-2 grids. Excluding the points that are also included in the 6D-3 grid, the root-mean-square deviations are 2.69 cm^{-1} (2D, 227 comparisons) and 0.62 cm^{-1} (6D-2, 544 comparisons), and the corresponding maximum deviations are 8.49 cm^{-1} (2D) and 2.23 cm^{-1} (6D-2). The agreement between computed CBS+ and interpolated CBS* energies is particularly good close to equilibrium (deviations smaller than 2 cm^{-1} for NH distances between 0.97 and 1.07 Å). It should be stressed that the current approach does not allow for extrapolation where the cubic polynomials may produce meaningless results (checked for 2D). Inside the interpolation region, however, it appears to be reliable and to provide a high-level surface close to CBS+ quality.

It might be instructive to indicate the computational effort required to construct the surfaces by specifying the single-processor CPU times on a Compaq ES40 (833 MHz). About 4 min are needed for one ATZfc energy calculation, and hence the 6D PES and DMS on the large grid take about 40 and 240 days of the CPU time, respectively. To obtain the PES at the CBS+ level, most of CPU time is spent on the A5Zfc calculations (4 h CPU time per point, compared with 30 min per AQZfc point). Overall the CBS+ PES on the 2D, 6D-2, and 6D-3 grids (420, 560, and 700 points) take about 75, 100, and 125 days of CPU time, respectively.

For the sake of brevity, the 2D and 6D surfaces are not tabulated here. They have been fitted to analytical potential functions (Sec. III) and are well represented by a set of potential energy parameters (Sec. IV).

III. THE ANALYTICAL FUNCTION USED TO REPRESENT THE POTENTIAL ENERGY SURFACE

With the purpose of computing vibrational energies for ammonia and, by comparing the theoretical values to experiment, to determine the accuracy of the *ab initio* calculations, we have fitted a parameterized analytical function, which depends on all six vibrational coordinates of NH_3, through the *ab initio* points.

It is well known that the potential energy function for the inversion motion of NH_3 is strongly anharmonic with a relatively small barrier to planarity. Even in the vibrational states of lowest energy the molecule can tunnel through the barrier and access two equivalent minima on the potential energy surface. Because of the strong anharmonicity of this ''umbrella'' motion the description of it requires special consideration.

We describe first the coordinates used in the parameterized analytical function that represents the potential energy function. The protons in NH_3 are labeled as 1, 2, 3, and r_i denotes the instantaneous distance between the N nucleus and proton i. We express the dependence of the potential energy function on these stretching coordinates by an expansion in the Morse variables

$$\xi_i = 1 - \exp(-a(r_i - r_e)), \quad i = 1,2,3, \tag{2}$$

where r_e is the common equilibrium bond length for the three bonds, and a is a molecular parameter. By using the Morse variables in Eq. (2) rather than bond length displacements $r_i - r_e$ for expanding the potential energy function, we obtain faster convergence of the expansion. Also, when we use Morse oscillator eigenfunctions as stretching basis functions for the variational calculations, we have the advantage of being able to calculate the integrals over the r_i analytically

when setting up the matrix representation of the Hamiltonian.[24] We define the "interbond angle" α_1 as the angle between the $N-H_2$ and $N-H_3$ bonds (where, for example, by $N-H_2$ we mean the bond between the N nucleus and the proton labeled 2), α_2 is the angle between $N-H_1$ and $N-H_3$, and α_3 is the angle between $N-H_1$ and $N-H_2$. These three angles have the common equilibrium value α_e and we define $\Delta\alpha_i=\alpha_i-\alpha_e$. We form the following symmetrized combinations of the $\Delta\alpha_i$:

$$\xi_{4a}=\frac{1}{\sqrt{6}}(2\Delta\alpha_1-\Delta\alpha_2-\Delta\alpha_3), \tag{3}$$

$$\xi_{4b}=\frac{1}{\sqrt{2}}(\Delta\alpha_2-\Delta\alpha_3); \tag{4}$$

these two coordinates have E_1' symmetry in the molecular symmetry group $D_{3h}(M)$ (see pp. 41 and 85 of Ref. 1). We express the dependence of the potential energy function on the inversion angle through the quantity

$$\sin\overline{\rho}=\frac{2}{\sqrt{3}}\sin(\overline{\alpha}/2), \tag{5}$$

where

$$\overline{\alpha}=\tfrac{1}{3}(\alpha_1+\alpha_2+\alpha_3) \tag{6}$$

is the average of the instantaneous values of the three interbond angles α_i. If the molecular geometry has C_{3v} symmetry, then it is easy to show that $\overline{\rho}$ is the angle between the C_3 axis and any one of the bonds. In less symmetrical configurations there is no simple geometrical interpretation of $\overline{\rho}$, but $\sin\overline{\rho}$ can be easily determined in any configuration, and it is totally symmetric in the molecular symmetry group.

By analogy with the expansion used for triatomic molecules in Ref. 25, the parametrized analytical function used to represent the potential surface is chosen as

$$\begin{aligned}V(\xi_k;\sin\overline{\rho})=V_e+V_0(\sin\overline{\rho})+\sum_j F_j(\sin\overline{\rho})\xi_j\\ +\sum_{j\leq k}F_{jk}(\sin\overline{\rho})\xi_j\xi_k\\ +\sum_{j\leq k\leq l}F_{jkl}(\sin\overline{\rho})\xi_j\xi_k\xi_l\\ +\sum_{j\leq k\leq l\leq m}F_{jklm}(\sin\overline{\rho})\xi_j\xi_k\xi_l\xi_m+\cdots,\end{aligned} \tag{7}$$

where the five curvilinear internal coordinates ξ_k, $\{k=1,2,3,4a,4b\}$ are made up of the three local Morse variables (2) for $k=1$, 2, 3 and the degenerate bending symmetrized coordinates (3–4) for $k=4a$, $4b$ respectively. The expansion coefficients $F_{jk\ldots}(\sin\overline{\rho})$ depend on $\sin\overline{\rho}$; the inversion coordinate is the sixth internal coordinate needed for describing the vibrations of the ammonia molecule.

The pure inversion potential function is defined as

$$V_0(\sin\overline{\rho})=\sum_{s=1}^{5}f_0^{(s)}(\sin\rho_e-\sin\overline{\rho})^s; \tag{8}$$

and the expansion functions are

$$F_{jk\ldots}(\sin\overline{\rho})=\sum_{s=0}^{n}f_{jk\ldots}^{(s)}(\sin\rho_e-\sin\overline{\rho})^s, \tag{9}$$

where the parameter ρ_e is the equilibrium value of $\overline{\rho}$ in the C_{3v} symmetry equilibrium geometry, and n is chosen sufficiently large for the fitting of the *ab initio* points to be satisfactory. In our case, the *ab initio* data are well described with a potential of fifth order.

Our choice of the function $\sin\rho_e-\sin\rho$ to expand the coefficients $F_{jk\ldots}(\sin\overline{\rho})$ is based on the fact that $\sin\overline{\rho_e}-\sin\overline{\rho}$ attains its minimum value at planar geometries where $\alpha_1+\alpha_2+\alpha_3=2\pi$. Thus, our expansion for the potential energy function has a maximum or a minimum (i.e., the first derivative vanishes) at planar geometries as required by symmetry. Also, as mentioned above, $\sin\overline{\rho}$ is totally symmetric under the symmetry operations in $D_{3h}(M)$.

IV. POTENTIAL FUNCTION FITTING TO THE *AB INITIO* POINTS

We have chosen the following *ab initio* data sets as input for the fitting procedure: 6D-1-ATZfc (14 400 points), 6D-1-CBS* (14 400 points), and 6D-CBS+ (1 680 points; combination of all CBS+ points from 2D-CBS+, 6D-2-CBS+, and 6D-3-CBS+). The latter set covers only a relatively small grid of nuclear geometries, but all points are computed at the highest level applied presently. The former two sets cover the full 6D-PES, and the interpolated 6D-1-CBS* energies are expected to be almost as accurate as those from 6D-CBS+. Table IV lists the resulting potential energy parameters (that are allowed by symmetry and determined to be significantly different from zero) and the standard deviations of the fits: all values are given in cm^{-1} except for the equilibrium inversion coordinate ρ_e (in deg), the equilibrium bond length r_e (in Å), and the Morse parameter a (in $Å^{-1}$). In the case of 6D-1-ATZfc, the equilibrium geometry from the fitting procedure (Table IV) can be compared to that from direct optimization (Table I): the deviations are 0.000 037 Å for the bond length and 0.015° for the bond angle.

A total of 76 and 75 fit parameters were necessary for 6D-1-ATZfc and 6D-1-CBS*, respectively, to get a reasonable description of the full 6D-PES (14 400 points extending in energy up to 30 000 cm^{-1}), whereas 70 parameters were sufficient for the smaller 6D-CBS+ grid. In each case, the standard deviations of the fits were very small (4–5 cm^{-1}, see Table IV) indicating that the *ab initio* energies depend smoothly on the vibrational coordinates. However, some of the fitted parameters have quite different values for the various potential surfaces, especially for high order parameters. Consequently, we cannot estimate the accuracy of the *ab initio* calculation from the fitting of the points alone; this fitting only reflects the internal consistency of the data points. To determine this accuracy, it is necessary to carry out the vibrational calculations and compare the resulting theoretical vibrational energies with the corresponding experimental values.

The interpolation scheme leading to the 6D-1-CBS* surface is one way of using high-accuracy CBS+ information to correct 6D-1-ATZfc energies so that high-accuracy energies can be computed at a large number of nuclear geometries. We have also explored another way towards the same end. We have constructed an analytical potential sur-

TABLE IV. Potential energy parameters for the ground electronic state of NH_3.

	6D-1-ATZfc	6D-CBS+	6D-CBS*	6D-APS
ρ_e	112.375479(10)	112.092(20)	112.069(10)	112.0843(66)
r_e	1.014935(28)	1.010324(71)	1.0102908(27)	1.010337(15)
a^a	2.15	2.15	2.15	2.15
V_e	−12396051.17(15)	−12419378.49(28)	−12419378.72(14)	−12396051.17(15)
f_0^2	329195(53)	326006(122)	326679(43)	322858(479)
f_0^3	−486714(520)	−406028(1477)	−427230(519)	−416488(4304)
f_0^4	1069766(2985)	775804(9463)	862091(2820)	1315890(60941)
f_0^5				−2122063(213011)
f_1^1	−33988(10)	−33334(45)	−33571(10)	−33240(104)
f_1^2	52708(98)	44356(450)	47047(96)	44268(968)
f_1^3	−356836(1699)	−398530(6271)	−346854(1713)	−424252(15179)
f_1^4	545666(8839)	931886(32154)	567383(8644)	1040313(75844)
f_{11}^0	38157(22)	38847(22)	38755.2(18)	38727(16)
f_{11}^1	−18583(38)	−18348(296)	−18769(38)	−18155(451)
f_{11}^2	56381(380)	64442(1625)	55717(354)	76085(3187)
f_{11}^3	−242559(2506)	−320503(14073)	−237488(2356)	−430847(25523)
f_{13}^0	−412.7(22)	−492(22)	−422.6(22)	−412.7(22)
f_{13}^1	4875(32)	4553(201)	4820(31)	4875(32)
f_{13}^2	39890(420)	47606(1986)	40429(423)	39890(420)
f_{13}^3	−74434(2827)	−138784(17523)	−77362(2780)	−74434(2827)
f_{4a4a}^0	16940.4(34)	16817.2(92)	16780.5(28)	16940.4(34)
f_{4a4a}^1	64765(80)	67008(287)	67180(75)	64765(80)
f_{4a4a}^2	−111454(1994)	−88799(3005)	−86426(1507)	−111454(1994)
f_{4a4a}^3	376194(16352)	119595(35112)	88781(12643)	376194(16352)
$f_{14a}^0\sqrt{3}/\sqrt{2}$	−4472.5(61)	−4538(36)	−4405.3(59)	−4472.5(61)
$f_{14a}^1\sqrt{3}/\sqrt{2}$	−20100(118)	−20278(763)	−20530(114)	−20100(118)
$f_{14a}^2\sqrt{3}/\sqrt{2}$	−81498(2137)	−72748(8100)	−82266(1848)	−81498(2137)
$f_{14a}^3\sqrt{3}/\sqrt{2}$	298489(16068)	239150(62130)	274759(13280)	298489(16068)
f_{111}^0	655.4(37)	476(23)	509.9(34)	416(32)
f_{111}^1	−10043(85)	−11004(349)	−10539(80)	−13268(958)
f_{111}^2	22276(660)	40930(3270)	28679(654)	78837(10104)
f_{113}^0	−277.9(28)	−305(19)	−307.5(26)	−277.9(28)
f_{113}^1	1973(50)	1370(309)	1655(49)	1973(50)
f_{113}^2	10078(400)	22159(3574)	13188(400)	10078(400)
f_{123}^0	−243.7(88)	−348(76)	−236.2(82)	−243.7(88)
f_{123}^1	4432(144)	1151(1385)	4632(138)	4432(144)
f_{4a4a4a}^0	−406.4(67)	−456(17)	−529.6(54)	−406.4(67)
f_{4a4a4a}^1	20078(232)	16166(481)	18262(152)	20078(232)
f_{4a4a4a}^2	−25495(2800)		1323(783)	−25495(2800)
$f_{114a}^0\sqrt{3}/\sqrt{2}$	−2747(12)	−2905(69)	−2767(12)	−2747(12)
$f_{114a}^1\sqrt{3}/\sqrt{2}$	−13878(198)	−13450(990)	−14234(188)	−13878(198)
$f_{134b}^0\sqrt{2}$	−5040(16)	−5103(88)	−4994(15)	−5040(16)
$f_{134b}^1\sqrt{2}$	−17212(329)	−14198(1795)	−17526(297)	−17212(329)
$f_{134b}^2\sqrt{2}$	39323(3039)	65042(20322)	36781(2482)	39323(3039)
f_{14a4a}^0	−2261.3(43)	−2356(26)	−2356.6(43)	−2261.3(43)
f_{14a4a}^1	−9737(125)	−10335(541)	−9494(124)	−9737(125)
f_{14a4a}^2	−16225(1381)		−14168(1333)	−16225(1381)
$-f_{24a4b}^0/\sqrt{2}$	929(13)	1060(46)	897(11)	929(13)
$-f_{24a4b}^1/\sqrt{2}$	2791(340)		2698(190)	2791(340)
$-f_{24a4b}^2/\sqrt{2}$	−12839(3547)			−12839(3547)
f_{1111}^0	3379(15)	2729(159)	3546(15)	3547(154)
f_{1111}^1	−4388(267)	−6897(1960)	−4297(268)	−6526(3561)
f_{1113}^0	−420(11)	−333(87)	−487(11)	−420(11)
f_{1133}^0	−161(14)		−109(14)	−161(14)
f_{1133}^1	3915(249)	5693(2066)	3808(249)	3915(249)
f_{1123}^0	−182(14)	10(95)	−144(15)	−182(14)
f_{1123}^1	1215(244)	3372(2125)	969(247)	1215(244)
f_{114a4a}^0	−2292(29)	−1482(103)	−2049(27)	−2292(29)
f_{114a4a}^1	5913(533)		1736(507)	5913(533)
$-f_{224a4b}^0/\sqrt{2}$	1397(34)	1962(173)	1642(34)	1397(34)
$-f_{224a4b}^1/\sqrt{2}$	−6546(622)	−14853(3451)	−10368(611)	−6546(622)
f_{134a4a}^0	1252(30)	394(128)	968(28)	1252(30)
f_{134a4a}^1	−13899(563)	−9986(2492)	−10275(537)	−13899(563)
$-f_{134a4b}^0/\sqrt{2}$	886(47)	2078(247)	1320(45)	886(47)
$-f_{134a4b}^1/\sqrt{2}$	14669(908)	12526(4945)	8550(878)	14669(908)

TABLE IV. (*Continued*.)

	6D-1-ATZfc	6D-CBS+	6D-CBS*	6D-APS
$f^0_{1114a}\sqrt{3}/\sqrt{2}$	−1049(43)	−1069(257)	−1357(43)	−1049(43)
$f^1_{1114a}\sqrt{3}/\sqrt{2}$	−6390(651)	1131(4025)	−2978(647)	−6390(651)
$f^0_{4a4a4a4a}$	655(18)	829(41)	723(14)	655(18)
$f^1_{4a4a4a4a}$	13562(397)	6739(1128)	8850(306)	13562(397)
$f^0_{1134a}\sqrt{3}/\sqrt{2}$	2226(38)	3170(208)	2528(37)	2226(38)
$f^1_{1134a}\sqrt{3}/\sqrt{2}$	4398(604)	11087(4243)	1778(595)	4398(604)
$f^0_{1124b}\sqrt{2}$	2419(39)	2091(195)	2294(39)	2419(39)
$f^1_{1124b}\sqrt{2}$	−6483(709)	−1626(4386)	−3911(700)	−6483(709)
$f^0_{14a4a4a}$	316.2(93)	223(60)	260.6(93)	316.2(93)
$f^1_{14a4a4a}$	3581(181)	5178(1131)	4285(176)	3581(181)
$f^0_{24a4a4b}\sqrt{2}$	−1062(48)	−1813(147)	−1521(43)	−1062(48)
$f^1_{24a4a4b}\sqrt{2}$	−19739(934)	−16366(2784)	−13132(855)	−19739(934)
Standard deviation	4.6	4.3	4.3	5.7

[a]Obtained by means of a one-dimensional fitting of a stretching Morse potential to the *ab initio* points in the vicinity of the equilibrium geometry and kept fixed in the fitting of the other potential surfaces.

face 6D-APS by first fitting the analytical function in Eq. (7) to the 6D-1-ATZfc points and then to the 2D-CBS+ *ab initio* points. In the second fitting all parameters, which could not be reliably determined, were held fixed at the values obtained in the initial fit to the ATZfc points. Thus, in a sense, the CBS+ potential is superimposed on the ATZfc potential. In the 6D-APS potential, the information about the 2D pure symmetric stretching and bending motion is obtained from the CBS+ points, but the information about all other vibrational motions originates in the ATZfc points. Thus, when we leave the region in coordinate space with the CBS+ points, the potential energy function does not just extrapolate arbitrarily. Instead its behavior is governed by the ATZfc calculated points. The 6D-APS potential parameters are given in the last column of Table IV. To reach the standard deviation of 5.7 cm^{-1} with respect to the 2D-CBS+ potential energy surface it was necessary to include one parameter, f^5_0, in addition to those used in the other fittings.

V. VIBRATIONAL ENERGY CALCULATION

For the vibrational energy calculations we have developed a program XY3. This program is based on the Hougen–Bunker–Johns (HBJ) formalism[26] (see also Refs. 1 and 27) involving a nonrigid reference configuration that follows the large-amplitude inversion motion of the ammonia molecule. The other (small amplitude) vibrations are then measured as displacements from this reference configuration. In practical terms, in the HBJ approach the inversion motion is treated together with the rotation, and the inversion coordinate can be thought of as a fourth rotation angle.[26] We give here only a very brief outline of the theory developed to do the vibrational energy calculations;[28] more details will be given in a subsequent publication.

To get an expression for the nuclear kinetic energy in the HBJ formalism we choose the reference configuration for XH_3 type-molecules to have C_{3v} symmetry: the three bond lengths are held fixed at equal values r_e and the bond angles are equal but are allowed to vary. The components $\mathbf{a}_i(\rho)$ of the position vector for nucleus i (the protons are labeled 1, 2, 3, and the nitrogen nucleus is labeled 4) in the molecule-fixed axis system are obtained in Ref. 29. Here, we have introduced a new inversion coordinate ρ, and it is necessary to clarify its definition in order not to confuse it with the instantaneous inversion coordinate $\overline{\rho}$ employed to describe the potential energy function (see Fig. 1). The two inversion coordinates ρ and $\overline{\rho}$ are identical when the molecule is in the reference configuration with C_{3v} symmetry and all three bond lengths equal to r_e. If the molecule is distorted away from the reference configuration, it is possible to express $\overline{\rho}$ in terms of ρ and the other vibrational coordinates. For a given nuclear geometry, the instantaneous value of ρ is determined together with the instantaneous values of the Eckart angles θ, ϕ, χ used as rotational coordinates by solving four equations obtained from the Eckart[30] and Sayvetz[31] conditions.

For the kinetic energy the internal coordinates used are linearized at an arbitrary reference configuration[32] so that they approximate the curvilinear internal coordinates given in Eqs. (2)–(4),

$$\mathbf{S}^l = \sum_i B_i(\rho)\mathbf{d}_i, \tag{10}$$

where $\mathbf{d}_i$ is a three-component column vector describing the displacement of nucleus i from its reference position in the molecule-fixed axis system, $B_i(\rho)$ is a transformation matrix, and $\mathbf{S}^l$ is a five-dimensional column vector containing the linearized vibrational coordinates. This vector is defined as

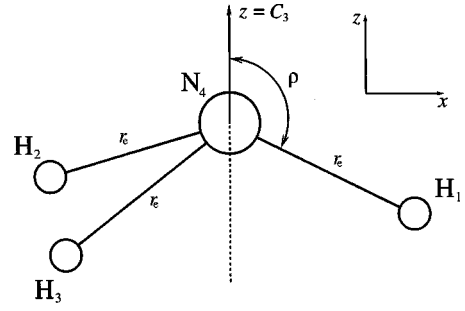

FIG. 1. Reference configuration chosen for ammonia. The origin of the molecule fixed axis system coincides with the center-of-mass.

$$(\mathbf{S}^l)^T=(\Delta r_1^l,\Delta r_2^l,\Delta r_3^l,S_{4a}^l,S_{4b}^l), \tag{11}$$

where the superscript T denotes transposition and

$$S_{4a}^l=\frac{1}{\sqrt{6}}(2\Delta\alpha_1^l-\Delta\alpha_2^l-\Delta\alpha_3^l), \tag{12}$$

$$S_{4b}^l=\frac{1}{\sqrt{2}}(\Delta\alpha_2^l-\Delta\alpha_3^l). \tag{13}$$

With this choice of coordinates we simplify the expression for the vibrational kinetic energy, which is obtained by performing a Sørensen procedure[33] with seven constraints: the fact that the molecule-fixed axis system has origin in the nuclear center-of-mass in conjunction with the Eckart[30] and Sayvetz[31] conditions.

As explained above, the potential energy function is expressed in terms of the three Morse variables in Eq. (2), which in turn depend on the instantaneous values of the three bond lengths, the two bending coordinates defined in Eqs. (3) and (4), and the ''instantaneous'' inversion coordinate $\overline{\rho}$ defined in Eqs. (5) and (6). These coordinates are all geometrically defined so that the parameters in the analytical expression for the potential energy function have the same values for all isotopomers of the molecule. The kinetic energy operator, on the other hand, is expressed in terms of $\{\Delta r_1^l,\Delta r_2^l,\Delta r_3^l,S_{4a}^l,S_{4b}^l,\rho\}$. To obtain the vibrational Hamiltonian we must carry out suitable coordinate transformations to ensure that the operators representing the kinetic and potential energies depend on the same coordinates. This is achieved by expanding the potential energy function in terms of linearized coordinates in Eq. (11) up to fourth order. Expansion coefficients are obtained numerically computing partial derivatives of the potential energy function with respect to linearized coordinates at the equilibrium geometry. The transformation does not simply lead to the potential function being expressed as a Taylor expansion in the linearized coordinates. We express it in terms of the Morse variables in Eq. (2) with bond length displacements r_i-r_e determined in terms of the linearized coordinates. Consequently, the potential energy function used in the vibrational Hamiltonian has the desirable properties resulting from the expansion in curvilinear coordinates: It approaches a constant value for long bond lengths, for example.

The energy calculations are performed by variationally diagonalizing a matrix representation of the inversion-vibrational Hamiltonian. This matrix representation is constructed in a basis set whose functions are obtained as products of (a) Morse oscillator functions for the local stretching modes; (b) two-dimensional isotropic harmonic oscillator functions for the bending modes described by $\{S_{4a}^l,S_{4b}^l\}$; and (c) inversion functions depending on ρ. The latter functions are obtained by numerically solving the one-dimensional inversion Schrödinger problem with the Numerov–Cooley method.[29,34–36]

The results of band center calculations for NH_3 and its isotopomers $^{15}NH_3$, NT_3, $^{15}ND_3$, and ND_3 together with observed data are given in Tables V–VII. In the tables we label the states in the ''standard'' spectroscopic notation, as they appear in experimental papers,[2,3,28,37–41] and in the local-mode notation. The quantum numbers in the local-mode notation are obtained as those for the basis function with the largest contribution (i.e., the largest absolute value of the eigenvector coefficient) to the eigenfunction. In the standard notation v_1 is the usual harmonic-oscillator quantum number for the totally symmetric stretching mode, v_2^p is the harmonic-oscillator quantum number for the inversion, and p is the parity of the inversion state in question, and $v_3^{l_3}$ and $v_4^{l_4}$ are the quantum numbers for the two-dimensional harmonic oscillator for the degenerate stretching and bending mode, respectively. For the local notation n_1, n_2, and n_3 are the local stretching quantum numbers, N_b and l describe the degenerate bending mode with l being the quantum number for the vibrational angular momentum, and n_i corresponds to the inversion mode.

By comparing the deviations between calculated and observed band centers in Table V, one can get an impression of the quality of the potential surfaces 6D-1-CBS*, 6D-CBS+, and 6D-APS. As discussed above (Sec. IV), the 6D-CBS+ surface is obtained by directly fitting one set of *ab initio* points computed at the highest level of theory employed in the present work, whereas the 6D-1-CBS* and 6D-APS surfaces result from the combination of the CBS+ and ATZfc data points. The calculated band centers in Table V document that all the potential surfaces considered are of high quality; the agreement with experiment is comparable for all of them (see also rms deviations in Table V) but best for the 6D-APS surface. Band center calculations have also been performed for the 6D-1-ATZfc surface (results not shown in Table V): as expected, the rms deviation of 34.0 cm^{-1} is larger here than in the other cases because of the exclusive use of data obtained with a smaller basis.

Due to strong interactions between states and to the fact that several calculated energies are often close to a given experimental energy, in some cases we could not establish a direct correspondence between experimental and calculated data. For this reason, only band centers with obvious assignments are reported in Table V. We could not determine an appropriate assignment for the vibrational polyad blocks $N=n_1+n_2+n_3+(N_b)/2=3,...,6$ as illustrated in Table VI, where we list the corresponding band centers. The calculation reported in this table has been done with the 6D-APS potential parameters. The largest contributions in local notation to the respective eigenvectors are also shown in Table VI and in some cases do not correspond to the standard assignments.[2] To obtain a correct assignment we must also compute the transitions intensities.

The band center values corresponding to the pure inversion $4\nu_2$ band require some comments. In 1984 Ziegler and Hudson[37] reported the values 3448 ± 5 cm^{-1} and 4045 ± 5 cm^{-1} for the band centers of the $4\nu_2^+$ and $4\nu_2^-$ states, respectively. However in 1999 Kleiner *et al.*[39] claimed a new value for the $4\nu_2^+$ around 3462 cm^{-1}, which is in good agreement with our calculation. Except for the $4\nu_2^-$ state, the calculated pure inversion band centers are very close to the experimental values. We calculate the term value of the $4\nu_2^-$ state to be 4067.39 cm^{-1}. For the states $v_2\nu_2$ in Table V whose energies are determined experimentally at high precision, the deviation from experiment is a few cm^{-1}. It seems

TABLE V. Experimental and calculated vibrational band centers for NH_3.

				6D-CBS+		6D-1-CBS*		6D-APS	
Γ	$v_1\ v_2^p\ v_3^{l_3}\ v_4^{l_4}$	$n_1\ n_2\ n_3\ N_b^l\ n_i$	Expt.[a]	Calc.	Expt.−Calc.	Calc.	Expt.−Calc.	Calc.	Expt.−Calc.
A_1'	$0\ 1^+\ 0^0\ 0^0$	$0\ 0\ 0\ 0^0\ 1$	932.43	936.92	−4.49	936.05	−3.62	934.77	−2.34
A_1'	$0\ 2^+\ 0^0\ 0^0$	$0\ 0\ 0\ 0^0\ 2$	1597.47[e]	1603.34	−5.87	1602.77	−5.30	1601.79	−4.32
A_1'	$0\ 3^+\ 0^0\ 0^0$	$0\ 0\ 0\ 0^0\ 3$	2384.15[f]	2385.33	−1.18	2385.75	−1.60	2383.14	1.01
A_1'	$0\ 0^+\ 0^0\ 2^0$	$0\ 0\ 0\ 2^0\ 0$	3216.02	3209.88	6.14	3201.16	14.86	3211.05	4.97
A_1'	$1\ 0^+\ 0^0\ 0^0$	$0\ 0\ 1\ 0^0\ 0$	3336.02	3336.70	−0.68	3337.33	−1.31	3338.97	−2.95
A_1'	$0\ 4^+\ 0^0\ 0^0$	$0\ 0\ 0\ 0^0\ 4$	3462[g,h]	3466.29	−4.29	3466.98	−4.98	3464.24	−2.24
A_1'	$0\ 1^+\ 0^0\ 2^0$	$0\ 0\ 0\ 2^0\ 1$	4115.62[d]	4109.18	6.44	4093.67	21.95	4095.66	19.96
A_1'	$1\ 1^+\ 0^0\ 0^0$	$0\ 0\ 1\ 0^0\ 1$	4294.51	4302.85	−8.34	4300.85	−6.34	4302.06	−7.55
A_1'	$1\ 0^+\ 0^0\ 2^0$	$0\ 0\ 1\ 2^0\ 0$	6520[c]	6524.01	−4.01	6518.16	1.84	6527.08	−7.08
A_1'	$2\ 0^+\ 0^0\ 0^0$	$0\ 0\ 2\ 0^0\ 0$	6606.0[c]	6590.88	15.12	6587.41	18.59	6591.77	14.23
A_1'	$0\ 0^+\ 2^0\ 0^0$	$0\ 1\ 1\ 0^0\ 0$	6795.3[c]	6793.20	2.10	6791.87	3.43	6788.45	6.85
A_1'	$0\ 0^+\ 3^0\ 0^0$	$1\ 1\ 1\ 0^0\ 0$	10232.52[c]	10244.41	−11.89	10234.35	−1.83	10230.09	2.43
A_1'	$5\ 0^+\ 0^0\ 0^0$	$0\ 0\ 5\ 0^0\ 0$	15450.82[c]	15425.97	24.85	15438.07	12.75	15445.50	5.32
E_1'	$0\ 0^+ 0^0\ 1^1$	$0\ 0\ 0\ 1^1\ 0$	1626.28[e]	1619.33	6.95	1615.15	11.13	1621.00	5.28
E_1'	$0\ 1^+\ 0^0\ 1^1$	$0\ 0\ 0\ 1^1\ 1$	2540.53[f]	2536.82	3.71	2530.14	10.39	2532.24	8.29
E_1'	$0\ 0^+\ 0^0\ 2^2$	$0\ 0\ 0\ 2^2\ 0$	3240.18	3225.14	15.04	3216.05	24.13	3227.14	13.04
E_1'	$0\ 0^+\ 1^1\ 0^0$	$0\ 0\ 1\ 0^0\ 0$	3443.68[g]	3443.97	−0.29	3442.14	1.54	3440.10	3.58
E_1'	$0\ 1^+\ 1^1\ 0^0$	$0\ 0\ 1\ 0^0\ 1$	4416.91	4423.10	−6.19	4419.24	−2.33	4417.73	−0.82
E_1'	$1\ 0^+\ 0^0\ 1^1$	$0\ 0\ 1\ 1^1\ 0$	4955.85[c]	4950.01	5.84	4945.30	10.55	4953.55	2.30
E_1'	$0\ 0^+\ 1^1\ 1^1$	$0\ 0\ 1\ 1^1\ 0$	5052.60[c]	5037.74	14.86	5029.99	22.61	5033.08	19.52
E_1'	$0\ 1^+\ 1^1\ 1^1$	$0\ 0\ 1\ 1^1\ 1$	6012.90[c]	5999.01	13.89	5987.30	25.60	5988.76	24.14
E_1'	$1\ 0^+\ 0^0\ 2^2$	$0\ 0\ 1\ 2^2\ 0$	6566.22[c]	6545.79	20.43	6535.84	30.38	6548.61	17.61
E_1'	$1\ 0^+\ 1^1\ 0^0$	$0\ 0\ 2\ 0^0\ 0$	6608.83[c]	6597.26	11.57	6588.50	20.33	6594.38	14.45
E_1'	$0\ 0^+\ 1^1\ 2^{-2}$	$0\ 0\ 1\ 2^2\ 0$	6677.23[c]	6664.48	12.75	6657.93	19.30	6660.27	16.96
E_1'	$0\ 0^+\ 2^2\ 0^0$	$0\ 1\ 1\ 0^0\ 0$	6850.20[c]	6851.87	−1.67	6847.93	2.27	6844.27	5.93
E_1'	$2\ 0^+\ 0^0\ 1^1$	$0\ 0\ 2\ 1^1\ 0$	8200[c]	8213.84	−13.84	8203.59	−3.59	8211.59	−11.59
E_1'	$0\ 0^+\ 3^1\ 0^0$	$0\ 1\ 2\ 0^0\ 0$	10110.86[c]	10098.24	12.62	10093.73	17.13	10112.69	−1.83
E_1'	$3\ 0^+\ 1^1\ 0^0$	$0\ 0\ 4\ 0^0\ 0$	12675.5[c]	12645.69	29.81	12653.05	22.45	12654.68	20.82
E_1'	$4\ 0^+\ 1^1\ 0^0$	$0\ 0\ 5\ 0^0\ 0$	15451.19[c]	15472.90	−21.71	15439.33	11.86	15461.37	−10.18
A_1''	$0\ 0^-\ 0^0\ 0^0$	$0\ 0\ 0\ 0^0\ 0$	0.79	0.74	0.05	0.76	0.03	0.74	0.05
A_1''	$0\ 1^-\ 0^0\ 0^0$	$0\ 0\ 0\ 0^0\ 1$	968.12	971.32	−3.20	970.80	−2.68	968.97	−0.85
A_1''	$0\ 2^-\ 0^0\ 0^0$	$0\ 0\ 0\ 0^0\ 2$	1882.18[e]	1882.79	−0.61	1882.62	−0.44	1880.22	1.96
A_1''	$0\ 3^-\ 0^0\ 0^0$	$0\ 0\ 0\ 0^0\ 3$	2895.51[f]	2894.65	0.86	2894.87	0.64	2892.33	3.18
A_1''	$0\ 0^-\ 0^0\ 2^0$	$0\ 0\ 0\ 2^0\ 0$	3217.59	3211.01	6.58	3202.38	15.21	3212.27	5.32
A_1''	$1\ 0^-\ 0^0\ 0^0$	$0\ 0\ 1\ 0^0\ 0$	3337.08	3337.53	−0.45	3338.18	−1.10	3339.81	−2.73
A_1''	$0\ 4^-\ 0^0\ 0^0$	$0\ 0\ 0\ 0^0\ 4$	4045[b]	4068.95	−23.95	4069.22	−24.22	4067.39	−22.39
A_1''	$0\ 1^-\ 0^0\ 2^0$	$0\ 0\ 0\ 2^0\ 1$	4173.25[d]	4153.24	20.01	4140.08	33.17	4143.47	29.78
A_1''	$1\ 1^-\ 0^0\ 0^0$	$0\ 0\ 1\ 0^0\ 1$	4320.06	4329.37	−9.31	4328.30	−8.24	4328.63	−8.57
A_1''	$0\ 0^-\ 2^0\ 0^0$	$0\ 1\ 1\ 0^0\ 0$	6796.73[c]	6788.79	7.94	6788.22	8.51	6784.73	12.00
A_1''	$0\ 0^-\ 3^3\ 0^0$	$1\ 1\ 1\ 0^0\ 0$	10234.73[c]	10230.76	3.97	10224.81	9.92	10219.59	15.14
A_1''	$5\ 0^-\ 0^0\ 0^0$	$0\ 0\ 5\ 0^0\ 0$	15447.38[c]	15436.30	11.08	15433.91	13.47	15446.90	0.48
E_1''	$0\ 0^-\ 0^0\ 1^1$	$0\ 0\ 0\ 1^1\ 0$	1627.37[e]	1620.21	7.16	1616.05	11.32	1621.91	5.46
E_1''	$0\ 1^-\ 0^0\ 1^1$	$0\ 0\ 0\ 1^1\ 1$	2586.13[f]	2575.62	10.51	2569.78	16.35	2571.94	14.19
E_1''	$0\ 0^-\ 0^0\ 2^2$	$0\ 0\ 0\ 2^2\ 0$	3241.61	3226.14	15.47	3217.08	24.53	3228.14	13.47
E_1''	$0\ 0^-\ 1^1\ 0^0$	$0\ 0\ 1\ 0^0\ 0$	3443.99[g]	3440.10	3.89	3437.87	6.12	3436.08	7.91
E_1''	$0\ 1^-\ 1^1\ 0^0$	$0\ 0\ 1\ 0^0\ 1$	4435.4	4438.26	−2.86	4434.98	0.42	4432.78	2.62
E_1''	$1\ 0^-\ 0^0\ 1^1$	$0\ 0\ 1\ 1^1\ 0$	4956.79[c]	4951.00	5.79	4946.32	10.47	4954.55	2.24
E_1''	$0\ 0^-\ 1^1\ 1^1$	$0\ 0\ 1\ 1^1\ 0$	5052.97[c]	5028.49	24.48	5019.62	33.35	5022.25	30.72
E_1''	$0\ 1^-\ 1^1\ 1^1$	$0\ 0\ 1\ 1^1\ 1$	6037.12[c]	6011.44	25.68	6000.92	36.20	6001.81	35.31
E_1''	$1\ 0^-\ 0^0\ 2^2$	$0\ 0\ 1\ 2^2\ 0$	6566.22[c]	6547.07	19.15	6537.13	29.09	6549.97	16.25
E_1''	$1\ 0^-\ 1^1\ 0^0$	$0\ 0\ 2\ 0^0\ 0$	6609.66[c]	6588.12	21.54	6592.07	17.59	6596.87	12.79
E_1''	$0\ 0^-\ 1^1\ 2^{-2}$	$0\ 0\ 1\ 2^2\ 0$	6677.95[c]	6668.19	9.76	6657.49	20.46	6660.67	17.28
E_1''	$0\ 0^-\ 2^2\ 0^0$	$0\ 1\ 1\ 0^0\ 0$	6850.70[c]	6850.07	0.63	6845.44	5.26	6842.75	7.95
E_1''	$0\ 0^-\ 3^1\ 0^0$	$0\ 1\ 2\ 0^0\ 0$	10111.31[c]	10092.49	18.82	10094.64	16.67	10118.33	−7.02
E_1''	$3\ 0^-\ 1^1\ 0^0$	$0\ 0\ 4\ 0^0\ 0$	12675.5[c]	12646.87	28.63	12652.78	22.72	12655.96	19.54
E_1''	$4\ 0^-\ 1^1\ 0^0$	$0\ 0\ 5\ 0^0\ 0$	15448.7[c]	15477.48	−28.78	15437.99	10.71	15455.05	−6.35
rms				13.6		16.1		13.0	

[a]The experimental energies are taken from Ref. 28, except where otherwise indicated.
[b]From Refs. 37, 38.
[c]From Ref. 2.
[d]From Ref. 4.
[e]From Ref. 40.
[f]From Ref. 3.
[g]From Ref. 39.
[h]From Ref. 41.

TABLE VI. Ambiguous assignments of the calculated band centers for NH_3.

N[a]	Γ	$v_1\ v_2^p\ v_3^{l_3}\ v_4^{l_4}$	Expt.[b]	Calc.	$\Psi=\Sigma_{\ldots}C^{n_1n_2n_3}_{N_b^l n_i}\lvert n_1\rangle\lvert n_2\rangle\lvert n_3\rangle\lvert N_b^l\rangle\lvert n_i\rangle$
3	E_1'	$1\ 0^+\ 0^0\ 4^2$	9 639.65	9 621.62	$0.93\lvert1\rangle\lvert1\rangle\lvert0\rangle\lvert2^2\rangle\lvert0\rangle+0.11\lvert0\rangle\lvert0\rangle\lvert1\rangle\lvert0^0\rangle\lvert6\rangle+\cdots$
				9 654.22	$0.78\lvert0\rangle\lvert0\rangle\lvert2\rangle\lvert2^0\rangle\lvert0\rangle+0.34\lvert0\rangle\lvert0\rangle\lvert2\rangle\lvert2^0\rangle\lvert1\rangle+\cdots$
				9 681.23	$0.90\lvert0\rangle\lvert0\rangle\lvert1\rangle\lvert4^4\rangle\lvert0\rangle+0.20\lvert1\rangle\lvert1\rangle\lvert0\rangle\lvert1^1\rangle\lvert2\rangle+\cdots$
		$2\ 0^+\ 1^1\ 0^0$	9 689.84	9 700.82	$0.92\lvert0\rangle\lvert0\rangle\lvert1\rangle\lvert4^4\rangle\lvert0\rangle+0.17\lvert0\rangle\lvert0\rangle\lvert2\rangle\lvert2^2\rangle\lvert0\rangle+\cdots$
		$0\ 0^+\ 1^1\ 4^0$	9 738.15	9 718.55	$0.85\lvert0\rangle\lvert0\rangle\lvert3\rangle\lvert0^0\rangle\lvert0\rangle+0.38\lvert0\rangle\lvert0\rangle\lvert2\rangle\lvert2^2\rangle\lvert0\rangle+\cdots$
				9 740.21	$0.50\lvert0\rangle\lvert0\rangle\lvert2\rangle\lvert2^2\rangle\lvert0\rangle+0.49\lvert0\rangle\lvert0\rangle\lvert2\rangle\lvert1^1\rangle\lvert2\rangle+\cdots$
4	E_1'	$1\ 0^+\ 0^0\ 6^2$	12 628.20	12 615.09	$0.84\lvert0\rangle\lvert0\rangle\lvert3\rangle\lvert2^0\rangle\lvert0\rangle+0.22\lvert0\rangle\lvert0\rangle\lvert3\rangle\lvert2^0\rangle\lvert1\rangle+\cdots$
		$3\ 0^+\ 1^1\ 0^0$	12 675.50	12 654.68	$0.65\lvert0\rangle\lvert0\rangle\lvert4\rangle\lvert0^0\rangle\lvert0\rangle+0.19\lvert0\rangle\lvert0\rangle\lvert4\rangle\lvert0^0\rangle\lvert1\rangle+\cdots$
				12 709.57	$0.67\lvert0\rangle\lvert0\rangle\lvert4\rangle\lvert0^0\rangle\lvert0\rangle+0.52\lvert1\rangle\lvert1\rangle\lvert0\rangle\lvert1^1\rangle\lvert5\rangle+\cdots$
5.5–6				18 090.10	$0.66\lvert1\rangle\lvert1\rangle\lvert0\rangle\lvert7^1\rangle\lvert0\rangle+0.45\lvert1\rangle\lvert1\rangle\lvert3\rangle\lvert0^0\rangle\lvert1\rangle+\cdots$
	E_1'	$5\ 0^+\ 1^1\ 0^0$	18 109.47	18 098.38	$0.90\lvert0\rangle\lvert0\rangle\lvert6\rangle\lvert0^0\rangle\lvert0\rangle+0.35\lvert0\rangle\lvert0\rangle\lvert6\rangle\lvert0^0\rangle\lvert1\rangle+\cdots$
				18 101.88	$0.89\lvert1\rangle\lvert1\rangle\lvert2\rangle\lvert3^1\rangle\lvert0\rangle+0.23\lvert1\rangle\lvert1\rangle\lvert2\rangle\lvert3^1\rangle\lvert1\rangle+\cdots$
				18 115.23	$0.81\lvert2\rangle\lvert1\rangle\lvert0\rangle\lvert5^5\rangle\lvert0\rangle+0.27\lvert1\rangle\lvert1\rangle\lvert2\rangle\lvert2^0\rangle\lvert1\rangle+\cdots$
5.5–6				18 068.04	$0.73\lvert3\rangle\lvert2\rangle\lvert0\rangle\lvert1^1\rangle\lvert0\rangle+0.22\lvert3\rangle\lvert2\rangle\lvert0\rangle\lvert1^1\rangle\lvert1\rangle+\cdots$
	A_1'	$6\ 0^+\ 0^0\ 0^0$	18 109.47	18 098.17	$0.90\lvert0\rangle\lvert0\rangle\lvert6\rangle\lvert0^0\rangle\lvert0\rangle+0.35\lvert0\rangle\lvert0\rangle\lvert6\rangle\lvert0^0\rangle\lvert1\rangle+\cdots$
				18 112.81	$0.90\lvert1\rangle\lvert1\rangle\lvert3\rangle\lvert1^1\rangle\lvert0\rangle+0.28\lvert1\rangle\lvert1\rangle\lvert3\rangle\lvert1^1\rangle\lvert1\rangle+\cdots$
				18 150.00	$0.77\lvert1\rangle\lvert1\rangle\lvert0\rangle\lvert7^1\rangle\lvert0\rangle+0.53\lvert0\rangle\lvert0\rangle\lvert1\rangle\lvert9^7\rangle\lvert0\rangle+\cdots$

[a]N is a polyad block number $N=n_1+n_2+n_3+(N_B)/2$.
[b]Reference 2.

likely that the calculated energy for $4\nu_2^-$ should have a comparable deviation. Thus it is probably more accurate than the present, approximate experimental value of 4045 cm^{-1}. For the same reason we did not include in Table V the experimental data that appeared in Ref. 38, where they were referred to as ''private communication'' with L. D. Ziegler. These values are all lower than our predictions by 20–40 cm^{-1}. Besides, we do not include for the corresponding states with negative parity[2] in Table VI. They would only increase the size of the table without adding new information. These energies are 18 109.18 cm^{-1} for A_1'' symmetry together with 9 642.32, 9 689.72, 9 738.84, 12 628.2, and 18 107.56 cm^{-1} for E_1'' symmetry.

It is worth making a few points related to the comparison between experiment and the theoretical results for the NH_3 molecule. As the initial step in the calculations reported here, we computed the pure inversion energy levels from the pure inversion Hamiltonian by neglecting the interactions with the other vibrational modes. A considerable improvement was obtained when we introduced the vibration-inversion Hamiltonian. That means that the correct description of the vibration-inversion interaction is essential for a good reproduction of the pure inversion energies. This fact is in some sense related to the important interactions not only between the pure symmetric stretching and the inversion modes noted by Pesonen *et al.*,[5] but also between inversion and asymmetric bending modes.

Interestingly enough, for the majority of the pure vibrational states (for which the inversion mode is in its ground state) we obtain theoretical energies closer to experiment from the purely vibrational Hamiltonian (which neglects inversion motion) (see Table VIII) than from the complete vibration-inversion Hamiltonian (see Table V). Also, the assignment of the states in Table VI are straightforward when the inversion is neglected. Besides, for such states, the prediction by the purely vibrational Hamiltonian are too high relative to experiment; for the complete vibration-inversion Hamiltonian the predictions are too low.

The band centers for various isotopomers of ammonia have been calculated from the 6D-APS potential energy surface. Table VII shows that with the *ab initio* force constants of NH_3, the prediction of the experimental data is good. Clearly there is no large breakdown of the Born–Oppenheimer approximation in the electronic ground state of NH_3. Some experimental data cited in Ref. 38 have relatively low accuracy (± 50 cm^{-1}); these values are not useful for the comparison of our theoretical results with experiment and have not been included in the tables.

Table VII shows that the local quantum numbers for the $^{14}ND_3$ levels at 4887.29, 4938.44, and 4887.67 cm^{-1} and the $^{14}NT_3$ level at 2014.1 cm^{-1} are in disagreement with the ''standard'' notation. However the n quantum numbers of our assignment are consistent with the work of Kauppi and Halonen[42] who have calculated the vibrational energies of ammonia by considering only the small-amplitude vibrations (i.e., the vibrational modes other than the inversion mode).

VI. CONCLUSIONS

We report here extensive *ab initio* calculations of the potential energy surface for the electronic ground state of the ammonia molecule in conjunction with variational calculations of the vibrational energies. Even for a relative small molecule like NH_3, a very large number of *ab initio* points are required to characterize the potential energy surface in the region of configuration space accessible to the molecule at low or moderate vibrational excitation. To allow an accurate calculation of the rotation-vibration energies, the *ab initio* points must be generated at a high level of theory, and it becomes a formidable computational task to derive them. In the present work, we have explored two possible ways of overcoming this problem by combining *ab initio* points ob-

TABLE VII. Experimental and calculated vibrational band centers for isotopomers of NH_3.

Γ	$v_1\ v_2\ v_3^{l_3}\ v_4^{l_4}$	$n_1\ n_2\ n_3\ N_b^l\ n_i$	Expt.[a]	Calc.	Expt.−Calc.
		$^{14}ND_3$			
A_1'	$0\ 1^+\ 0^0\ 0^0$	$0\ 0\ 0\ 0^0\ 1$	745.6	745.55	0.05
A_1'	$0\ 2^+\ 0^0\ 0^0$	$0\ 0\ 0\ 0^0\ 2$	1359.0	1360.10	−1.10
A_1'	$0\ 3^+\ 0^0\ 0^0$	$0\ 0\ 0\ 0^0\ 3$	1830.0	1827.74	2.26
A_1'	$0\ 0^+\ 0^0\ 2^0$	$0\ 0\ 0\ 2^0\ 0$	2359	2358.92	0.08
A_1'	$1\ 0^+\ 0^0\ 0^0$	$1\ 0\ 0\ 0^0\ 0$	2420.05	2422.13	−2.08
A_1'	$0\ 4^+\ 0^0\ 0^0$	$0\ 0\ 0\ 0^0\ 4$	2482.0	2479.32	2.68
A_1'	$0\ 1^+\ 0^0\ 2^0$	$1\ 0\ 0\ 0^0\ 1$	3093.01	3087.99	5.02
A_1'	$1\ 1^+\ 0^0\ 0^0$	$0\ 0\ 0\ 2^0\ 1$	3171.89	3174.67	−2.78
E_1'	$0\ 0^+\ 0^0\ 1^1$	$0\ 0\ 0\ 1^1\ 0$	1191.0	1190.05	0.95
E_1'	$0\ 0^+\ 1^1\ 0^0$	$1\ 0\ 0\ 0^0\ 0$	2563.96	2564.91	−0.95
E_1'	$0\ 1^+\ 1^1\ 0^0$	$1\ 0\ 0\ 0^0\ 1$	3327.94	3329.96	−2.02
E_1'	$0\ 0^+\ 1^1\ 2^0$	$2\ 0\ 0\ 0^0\ 0$	4887.29	4887.07	0.22
E_1'	$1\ 0^+\ 1^1\ 0^0$	$1\ 0\ 0\ 2^0\ 0$	4938.44	4935.49	2.95
E_1'	$0\ 0^+\ 2^2\ 0^0$	$1\ 1\ 0\ 0^0\ 0$	5100.66	5097.45	3.21
A_1''	$0\ 0^-\ 0^0\ 0^0$	$0\ 0\ 0\ 0^0\ 0$	0.05	0.05	0.00
A_1''	$0\ 1^-\ 0^0\ 0^0$	$0\ 0\ 0\ 0^0\ 1$	749.15	748.97	0.18
A_1''	$0\ 2^-\ 0^0\ 0^0$	$0\ 0\ 0\ 0^0\ 2$	1429.0	1429.53	−0.53
A_1''	$0\ 3^-\ 0^0\ 0^0$	$0\ 0\ 0\ 0^0\ 3$	2106.6	2104.60	2.00
A_1''	$0\ 0^-\ 0^0\ 2^0$	$0\ 0\ 0\ 2^0\ 0$	2359	2359.03	−0.03
A_1''	$1\ 0^-\ 0^0\ 0^0$	$1\ 0\ 0\ 0^0\ 0$	2420.64	2422.19	−1.55
A_1''	$0\ 4^-\ 0^0\ 0^0$	$0\ 0\ 0\ 0^0\ 4$	2876.0	2870.17	5.83
A_1''	$0\ 1^-\ 0^0\ 2^0$	$0\ 0\ 0\ 2^0\ 1$	3099.46	3092.76	6.70
A_1''	$1\ 1^-\ 0^0\ 0^0$	$1\ 0\ 0\ 0^0\ 1$	3175.87	3177.75	−1.88
E_1''	$0\ 0^-\ 0^0\ 1^1$	$0\ 0\ 0\ 1^1\ 0$	1191.0	1190.11	0.89
E_1''	$0\ 0^-\ 1^1\ 0^0$	$1\ 0\ 0\ 0^0\ 0$	2563.96	2562.16	1.80
E_1''	$0\ 1^-\ 1^1\ 0^0$	$1\ 0\ 0\ 0^0\ 1$	3329.56	3334.85	−5.29
E_1''	$0\ 0^-\ 1^1\ 2^0$	$2\ 0\ 0\ 0^0\ 0$	4887.67	4884.76	2.91
E_1''	$1\ 0^-\ 1^1\ 0^0$	$1\ 0\ 0\ 2^0\ 0$	4938.44	4938.27	0.17
E_1''	$0\ 0^-\ 2^2\ 0^0$	$1\ 1\ 0\ 0^0\ 0$	5100.66	5098.62	2.04
		$^{15}NH_3$			
A_1'	$0\ 1^+\ 0^0\ 0^0$	$0\ 0\ 0\ 0^0\ 1$	928.46	930.88	−2.42
A_1'	$0\ 2^+\ 0^0\ 0^0$	$0\ 0\ 0\ 0^0\ 2$	1591.19	1595.64	−4.45
A_1'	$0\ 3^+\ 0^0\ 0^0$	$0\ 0\ 0\ 0^0\ 3$	2369.32	2368.45	0.87
A_1'	$1\ 1^+\ 0^0\ 0^0$	$1\ 0\ 0\ 0^0\ 1$	4288.0[4]	4296.00	−8.00
A_1''	$0\ 0^-\ 0^0\ 0^0$	$0\ 0\ 0\ 0^0\ 0$	0.76	0.71	0.05
A_1''	$0\ 1^-\ 0^0\ 0^0$	$0\ 0\ 0\ 0^0\ 1$	962.69	963.87	−0.98
A_1''	$0\ 2^-\ 0^0\ 0^0$	$0\ 0\ 0\ 0^0\ 2$	1870.86	1869.08	1.78
A_1''	$0\ 3^-\ 0^0\ 0^0$	$0\ 0\ 0\ 0^0\ 3$	2876.13	2872.96	3.17
A_1''	$1\ 1^-\ 0^0\ 0^0$	$1\ 0\ 0\ 0^0\ 1$	4312.3[4]	4321.55	−9.25
		$^{14}NT_3$			
A_1'	$0\ 1^+\ 0^0\ 0^0$	$0\ 0\ 0\ 0^0\ 1$	656.37	655.64	0.73
A_1'	$1\ 0^+\ 0^0\ 0^0$	$0\ 0\ 0\ 2^0\ 0$	2014.1	2015.95	−1.85
E_1'	$0\ 0^+\ 0^0\ 1^1$	$0\ 0\ 0\ 1^1\ 0$	996.28	997.12	−0.84
E_1'	$0\ 0^+\ 1^1\ 0^0$	$1\ 0\ 0\ 0^0\ 0$	2184.76	2184.27	0.49
A_1''	$0\ 0^-\ 0^0\ 0^0$	$0\ 0\ 0\ 0^0\ 0$	0.01	0.01	0.00
A_1''	$0\ 1^-\ 0^0\ 0^0$	$0\ 0\ 0\ 0^0\ 1$	657.19	656.42	0.77
A_1''	$1\ 0^-\ 0^0\ 0^0$	$0\ 0\ 0\ 2^0\ 0$	2014.1	2015.96	−1.86
E_1''	$0\ 0^-\ 0^0\ 1^1$	$0\ 0\ 0\ 1^1\ 0$	996.28	997.13	−0.85
E_1''	$0\ 0^-\ 1^1\ 0^0$	$1\ 0\ 0\ 0^0\ 0$	2184.76	2184.67	0.09
		$^{15}ND_3$			
A_1'	$0\ 1^+\ 0^0\ 0^0$	$0\ 0\ 0\ 0^0\ 1$	739.53	740.57	−1.04
A_1''	$0\ 0^-\ 0^0\ 0^0$	$0\ 0\ 0\ 0^0\ 0$	0.05	0.05	0.00
A_1''	$0\ 1^-\ 0^0\ 0^0$	$0\ 0\ 0\ 0^0\ 1$	742.78	743.69	−0.91

[a]Reference 28.

TABLE VIII. Five-dimensional calculations of the vibrational band centers for NH_3.

				6D-APS	
Γ	$v_1\ v_2^p\ v_3^{l_3}\ v_4^{l_4}$	$n_1\ n_2\ n_3\ N_b^l\ n_i$	Expt.[a]	Calc.	Expt.−Calc.
A_1	$0\ 0^\pm\ 0^0\ 2^0$	$0\ 0\ 0\ 2^0\ 0$	3 216.8	3 209.1	7.7
A_1	$1\ 0^\pm\ 0^0\ 0^0$	$0\ 0\ 1\ 0^0\ 0$	3 336.6	3 333.2	3.4
A_1	$1\ 0^\pm\ 0^0\ 2^0$	$0\ 0\ 1\ 2^0\ 0$	6 520.0	6 511.1	8.9
A_1	$2\ 0^\pm\ 0^0\ 0^0$	$0\ 0\ 2\ 0^0\ 0$	6 606.0	6 594.0	12.0
A_1	$0\ 0^\pm\ 2^0\ 0^0$	$0\ 1\ 1\ 0^0\ 0$	6 796.0	6 799.5	−3.5
A_1	$0\ 0^\pm\ 3^3\ 0^0$	$1\ 1\ 1\ 0^0\ 0$	10 233.6	10 259.8	−26.2
A_1	$5\ 0^\pm\ 0^0\ 0^0$	$0\ 0\ 5\ 0^0\ 0$	15 449.1	15 454.6	−5.5
A_1	$6\ 0^\pm\ 0^0\ 0^0$	$0\ 0\ 6\ 0^0\ 0$	18 109.3	18 106.9	2.4
E_1	$0\ 0^\pm\ 0^0\ 1^1$	$0\ 0\ 0\ 1^1\ 0$	1 626.8	1 625.5	1.3
E_1	$0\ 0^\pm\ 0^0\ 2^2$	$0\ 0\ 0\ 2^2\ 0$	3 240.9	3 236.6	4.3
E_1	$0\ 0^\pm\ 1^1\ 0^0$	$0\ 0\ 1\ 0^0\ 0$	3 443.8	3 443.0	0.8
E_1	$1\ 0^\pm\ 0^0\ 1^1$	$0\ 0\ 1\ 1^1\ 0$	4 956.3	4 954.4	1.9
E_1	$0\ 0^\pm\ 1^1\ 1^1$	$0\ 0\ 1\ 1^1\ 0$	5 052.8	5 037.1	15.7
E_1	$1\ 0^\pm\ 0^0\ 2^2$	$0\ 0\ 1\ 2^2\ 0$	6 566.2	6 554.6	11.7
E_1	$1\ 0^\pm\ 1^1\ 0^0$	$0\ 0\ 2\ 0^0\ 0$	6 609.2	6 589.2	20.0
E_1	$0\ 0^\pm\ 1^1\ 2^{-2}$	$0\ 0\ 1\ 2^2\ 0$	6 677.6	6 659.7	17.9
E_1	$0\ 0^\pm\ 2^2\ 0^0$	$0\ 1\ 1\ 0^0\ 0$	6 850.5	6 859.3	−8.8
E_1	$2\ 0^\pm\ 0^0\ 1^1$	$0\ 0\ 2\ 1^1\ 0$	8 200.0	8 216.7	−16.7
E_1	$1\ 0^\pm\ 0^0\ 4^2$	$0\ 0\ 1\ 4^0\ 0$	9 641.0	9 629.0	12.0
E_1	$2\ 0^\pm\ 1^1\ 0^0$	$0\ 0\ 3\ 0^0\ 0$	9 689.8	9 681.0	8.8
E_1	$0\ 0^\pm\ 1^1\ 4^0$	$0\ 0\ 1\ 4^2\ 0$	9 738.5	9 725.9	12.6
E_1	$0\ 0^\pm\ 3^1\ 0^0$	$0\ 1\ 2\ 0^0\ 0$	10 111.1	10 126.4	−15.3
E_1	$1\ 0^\pm\ 0^0\ 6^2$	$0\ 0\ 1\ 6^2\ 0$	12 628.2	12 628.0	0.2
E_1	$3\ 0^\pm\ 1^1\ 0^0$	$0\ 0\ 4\ 0^0\ 0$	12 675.5	12 653.7	21.8
E_1	$4\ 0^\pm\ 1^1\ 0^0$	$0\ 0\ 5\ 0^0\ 0$	15 449.9	15 454.9	−5.0
E_1	$5\ 0^\pm\ 1^1\ 0^0$	$0\ 0\ 6\ 0^0\ 0$	18 108.5	18 107.0	1.5

[a]References to experimental data are in Table V. The experimental values are obtained as the averages of the inversion-split vibrational energies.

tained at different levels of theory for constructing one surface. In the first approach, corrections were applied to the ATZfc *ab initio* points, which are calculated over the 14 400-point 6D-1 grid. The corrections were determined by the CBS+ results, which were calculated over the 700-point 6D-3 grid only. We denoted the corrected points as 6D-1-CBS*. In the second approach, we produced the 6D-APS surface by first fitting the analytical function in Eq. (7) to the 6D-1-ATZfc points and then to the 2D-CBS+ *ab initio* points, constraining in the second fitting all parameters, which could not be reliably determined, to the ATZfc values. Table V shows that the root-mean-square deviation between experimental and theoretical band centers is 16.1 cm^{-1} for the 6D-1-CBS* surface and 13.0 cm^{-1} for the 6D-APS surface. The rms deviation for the 6D-CBS+ surface, where the points are calculated over the smaller 2D, 6D-2, and 6D-3 grids, is 13.6 cm^{-1}. That is, in the present case, the ''refitting'' procedure leading to the 6D-APS surface produces better vibrational energies than the interpolation scheme leading to the 6D-1-CBS* points. This is perhaps slightly surprising since in the construction of the 6D-1-CBS* points, we seek to obtain CBS+ accuracy at all the 14 400 points of the 6D-1 grid by interpolating to these geometries the difference between the ATZfc and CBS+ energies calculated at the 700 points of the 6D-3 grid. In the construction of the 6D-APS surface, we are making a less transparent improvement of the analytical PES by fitting as many parameters as we can from the high-accuracy 2D-CBS+ points which are located chiefly along the minimum energy path for inversion. The energy in other regions of configuration space are ''sacrificed'' in that they are determined from the lower-accuracy ATZfc points. It is fair to say that for all of the potential

surfaces employed here, the agreement with experiment of the vibrational energies is very good, the typical deviation being significantly less than 1%. The slightly lower rms deviation obtained with the 6D-APS surface relative to the 6D-1-CBS* surface may well be fortuitous and thus not indicative of any real difference in the quality between the two surfaces. It should also be mentioned that the *ab initio* potential energy surface calculated in the present work gives a significantly better reproduction of the experimental vibrational energies than obtained previously in *ab initio* calculations. For example, we reproduce here the experimental fundamental energies to within 7.9 cm^{-1} as compared with 15 cm^{-1} for Ref. 6.

In the course of calculating the vibrational energies, we have demonstrated the importance of asymmetric bending-inversion interaction for describing accurately the pure inversion states. Consideration of only the totally symmetric stretching modes together with the inversion is inadequate for a precise calculation of the term values of the pure inversion states.

As mentioned above, the model for the vibrational motion of NH_3 developed here is variational, but employs an Eckart-frame kinetic energy operator (see, for example, Ref. 1). This model is a first step towards a theoretical procedure for the variational calculation of rotation-vibration energies of ammonia. It is hoped that with such a procedure, which minimizes rotation-vibration interaction, highly excited rotational states of XY_3 molecules can be studied; such states will perhaps exhibit interesting behavior similar to the ''four fold energy cluster formation'' that takes place in some XH_2 molecules.[43]

Note added in proof. After submission, we became aware of three other relevant papers.[44–46]

ACKNOWLEDGMENTS

This work is supported by the European Commission through Contract No. HPRN-CT-2000-00022, ''Spectroscopy of Highly Excited Rovibrational States.''

[1] P. R. Bunker and P. Jensen, *Molecular Symmetry and Spectroscopy*, 2nd ed. (NRC Research, Ottawa, 1998).
[2] S. L. Coy and K. K. Lehmann, Spectrochim. Acta, Part A **45A**, 47 (1989).
[3] I. Kleiner, G. Tarrago, and L. R. Brown, J. Mol. Spectrosc. **173**, 120 (1995).
[4] V. Špirko and W. P. Kraemer, J. Mol. Spectrosc. **133**, 331 (1989).
[5] J. Pesonen, A. Miani, and L. Halonen, J. Chem. Phys. **115**, 1243 (2001).
[6] C. Leonard, N. C. Handy, S. Carter, and J. M. Bowman, Spectrochim. Acta, Part A **58A**, 825 (2002).
[7] A. G. Császár, W. D. Allen, and H. F. Schaefer III, J. Chem. Phys. **108**, 9751 (1998).
[8] W. Klopper, C. C. M. Samson, G. Tarczay, and A. G. Császár, J. Comput. Chem. **22**, 1306 (2001).
[9] J. M. L. Martin, T. J. Lee, and P. R. Taylor, J. Chem. Phys. **97**, 8361 (1992).
[10] N. C. Handy, S. Carter, and S. M. Colwell, Mol. Phys. **96**, 477 (1999).
[11] G. D. Purvis and R. J. Bartlett, J. Chem. Phys. **76**, 1910 (1982).
[12] M. Urban, J. Noga, S. J. Cole, and R. J. Bartlett, J. Chem. Phys. **83**, 4041 (1985).
[13] K. Raghavachari, G. W. Trucks, J. A. Pople, and M. Head-Gordon, Chem. Phys. Lett. **157**, 479 (1989).
[14] MOLPRO2000 is a package of *ab initio* programs written by H.-J. Werner and P. J. Knowles, with contributions from R. D. Amos, A. Bernhardsson, A. Berning *et al.*
[15] C. Hampel, K. Peterson, and H.-J. Werner, Chem. Phys. Lett. **190**, 1 (1992), and references therein. The program to compute the perturbative triples corrections has been developed by M. J. O. Deegan and P. J. Knowles, *ibid.* **227**, 321 (1994).
[16] T. H. Dunning, J. Chem. Phys. **90**, 1007 (1989).
[17] D. E. Woon and T. H. Dunning, J. Chem. Phys. **98**, 1358 (1993).
[18] Thresholds in atomic units: Primitive atomic orbital (AO) integrals are neglected if the exponential factor is below 10^{-14}. Contracted AO and symmetry AO (SO) integrals are neglected if they are less than 10^{-14}. Convergence criteria for HF calculations: 10^{-10} for density and 10^{-7} for energy; for CCSD(T) calculations: 10^{-10} for energy and 10^{-10} for coefficients; and for geometry optimization: 10^{-5} for gradient and 10^{-8} for energy.
[19] D. Feller, J. Chem. Phys. **96**, 6104 (1992); **98**, 7059 (1993).
[20] T. Helgaker, W. Klopper, H. Koch, and J. Noga, J. Chem. Phys. **106**, 9639 (1997).
[21] T. van Mourik, G. J. Harris, O. L. Polyansky, J. Tennyson, A. G. Császár, and P. J. Knowles, J. Chem. Phys. **115**, 3706 (2001).
[22] The interpolation method was tested for the planar D_{3h} configurations using ATZfc, AQZfc, and A5Zfc. The resulting N–H bond lengths were 0.997 554, 0.996 018, and 0.995 577 Å, respectively. They deviate from the directly optimized bond lengths in Table I by only +0.000 025, −0.000 006, and −0.000 020 Å, respectively. This indicates the precision of the interpolation. The corresponding deviations in the total energies are +0.000 029, +0.000 028, and +0.000 047 a.u., respectively.
[23] The bond length takes the following values: [0.60, 0.70, 0.80, 0.85, 0.90, 0.95, 0.97, 0.99, 1.01, 1.03, 1.05, 1.07, 1.09, 1.11, 1.15, 1.20, 1.25, 1.35, 1.45, 1.55, 1.65] Å. The angle takes the following values (the same as those in 1D-PES): [120, 119, 118, 116, 114, 112, 110, 109, 108, 107, 106, 105, 104, 103, 101, 99, 95, 90, 80, 70] deg.
[24] R. Lemus and A. Frank, Chem. Phys. Lett. **349**, 471 (2001).
[25] P. Jensen, J. Mol. Spectrosc. **128**, 478 (1988).
[26] J. T. Hougen, P. R. Bunker, and J. W. C. Johns, J. Mol. Spectrosc. **34**, 136 (1970).
[27] D. Papoušek and M. R. Aliev, *Molecular Vibrational-Rotational Spectra* (Elsevier, Amsterdam, 1982).
[28] V. Špirko, J. Mol. Spectrosc. **101**, 30 (1983).
[29] D. Papoušek, J. M. R. Stone, and V. Špirko, J. Mol. Spectrosc. **48**, 17 (1973).
[30] C. Eckart, Phys. Rev. **47**, 552 (1935).
[31] A. Sayvetz, J. Chem. Phys. **7**, 383 (1939).
[32] A. R. Hoy, I. M. Mills, and G. Strey, Mol. Phys. **24**, 1265 (1972).
[33] G. O. Sørensen, in *Topics in Current Chemistry*, edited by M. J. S. Dewar *et al.* (Springer-Verlag, Heidelberg, 1979), Vol. 82, p. 99.
[34] P. Jensen, Comput. Phys. Rep. **1**, 1 (1983).
[35] B. Numerov, Publs. Observatoire Central. Astrophys. Russ. **2**, 188 (1933).
[36] J. W. Cooley, Math. Comput. **15**, 363 (1961).
[37] L. D. Ziegler and B. Hudson, J. Phys. Chem. **88**, 1110 (1984).
[38] P. Rosmus, P. Botschwina, H. J. Werner, V. Vaida, P. C. Engelking, and M. I. McCarthy, J. Chem. Phys. **86**, 6677 (1987).
[39] I. Kleiner, L. R. Brown, G. Tarrago, Q-L. Kou, N. Picqué, G. Guelachvili, V. Dana, and J-Y. Mandin, J. Mol. Spectrosc. **193**, 46 (1999).
[40] C. Cottaz, I. Kleiner, G. Tarrago, L. R. Brown, J. S. Margolis, R. L. Poynter, H. M. Pickett, T. Fouchet, P. Drossart, and E. Lellouch, J. Mol. Spectrosc. **203**, 285 (2000).
[41] C. Cottaz, G. Tarrago, I. Kleiner, and L. R. Brown, J. Mol. Spectrosc. **209**, 30 (2001).
[42] E. Kauppi and L. Halonen, J. Chem. Phys. **103**, 6861 (1995).
[43] P. Jensen, G. Osmann, and I. N. Kozin, in *Vibration-Rotational Spectroscopy and Molecular Dynamics, Advanced Series in Physical Chemistry*, edited by D. Papoušek (World Scientific, Singapore, 1997), Vol. 9.
[44] M. Snels, L. Fusina, H. Hollenstein, and M. Quack, Mol. Phys. **98**, 837 (2000).
[45] D. Luckhaus, J. Chem. Phys. **113**, 1329 (2000).
[46] T. Rajamäki, A. Miani, J. Pesonen, and L. Halonen, Chem. Phys. Lett. **363**, 226 (2002).